INSTITUTE OF PLASMA PHYSICS

NAGOYA UNIVERSITY

RESEARCH REPORT

NAGOYA, JAPAN

Heating of High z Plasma by Laser

H. B. Kang, T. Yamanaka*, M. Waki*,
K. Yoshida*, Y. Sakagami** and C. Yamanaka*

IPPJ-142 October 1972

Further communication about this report is to be sent to the Research Information Center, Institute of Plasma Physics, Nagoya University, Nagoya, Japan.

Submitted to Journal of the Physical Society of Japan.

Permanent Adress:

* Faculty of Engineering, Osaka University, Osaka.

** Faculty of Engineering, Gifu University, Gifu.

Abstract

The properties of plasmas produced by high power laser were investigated. The laser beam was irradiated on the various targets of beryllium Be, carbon C and polyethylene $(CH_2)_n$ of high z number. The influence of the charge number z to the heating of the plasma was discussed.

The electron temperatures of plasmas form different targets were estimated by the measurement of soft x-ray.

The time variations of the reflected laser light from plasma were also investigated.

From the time of flight measurements with a Faraday cage and an electrostatic energy analyser, the different charged ions could be seperated and ion temperatures and drift velocities were obtained from their velocity profiles.

No influence of laser pulse duration to the temperature was observed in the cases of durations 2 ns, 4 ns and 10 ns.

The experimental results for fast rising laser pulse were discussed and compared with those for slow rising one.

1. Introduction

As high power glass lasers have an ability to deliver a large amount of energy very rapidly to matter, one can produce plasmas of high density and high temperature.

Many researchers have studied the mechanism of ionization, heating and hydrodynamic expansion of plasma by focusing laser beam on the solid surface in vacuum theoretically and experimentally. The kinetic energy of ions was determined either by the time of flight measurement or with the electrostatic energy analyzer.[1,2,3] Observation on the plasma radiation in time and space with high speed photographic technique and interferometric method have yielded the informations about the expansion rate and the density.[4,5] As the expansion of the plasma takes place after the heating relaxation, the supplied energy leaks to the surroundings. In order to produce high temperature and high density plasma the effective heating must be performed before the expansion starts. Therefore, rapidly rising laser pulse is essential for these experiments.

We used a nano-second laser beam to the several species of targets; beryllium Be, carbon C and polyethylene $(CH_2)_n$. The properties of high z plasma have been clarified.

2. Experimental Arrangement

The glass laser system to produce plasma, which has been developed by the authors, consisted of an oscillator, a pulse-forming system and a five stage of amplifiers. Fast rising laser pulses (rise time 1 ns) with variable pulse

width (1 ∿ 30 ns) were generated from a Q-switched laser using external pulse transmission mode (PTM) method which was composed of a laser triggered spark gap (L.T.S.G.), a KDP Pockels cell and Gran prisms.[6] Pulse-formed output of the oscillator was amplified up to 7 Joules* by the amplifier. The beam divergence of laser light was less than 1 mrad. The laser beam was focused onto the target in a vacuum chamber by lens of focal length 150 mm.

The various kinds of diagnostics were prepared to study the properties of laser-produced plasma. Electron temperature was obtained from the x-ray measurement.[7] Ion energy, number density and temperature were measured by the time of flight with a Faraday cage and an electrostatic energy analyzer. Incident and reflected laser lights from the target were also measured.

The experimental arrangement is shown schematically in Fig.1.

3. Experimental Procedures and Results

(1) Electron temperature measurement by the x-ray.[8]

Electron temperatures were estimated by measuring the intensity ratio of soft x-ray which transmitted through beryllium absorbers of different thickness (25 μ, 50 μ, 100 μ). The plastic scintillator with the neutral density filters and the photomultiplier (HTV-R292) were usded as shown in Fig.2. Assuming Maxwellian distribution of elec-

---

* At present laser output reaches up to more than 40 J for 2 ns pulse width.

trons, the total intensity I of bremsstrahlung is

$$I \sim n_e n_i z^2 T_e^{1/2} \quad . \tag{1}$$

The intensity I_E of the bremsstrahlung which has a photon energy of $E = h\nu$, is given by

$$I_E = C \frac{n_e n_i z^2}{(kT_e)^{1/2}} g_{ff} \exp(-\frac{E}{kT_e}), \tag{2}$$

where n_e, n_i are electron and ion density, respectively and z, T_e are charge number and electron temperature, respectively and g_{ff} is Gaunt factor.

The intensity I_E' of x-ray transmitted through a metal foil of absorption coefficient K(E) and thickness D_n is given by

$$I_E' = C \frac{n_e n_i z^2}{(kT_e)^{1/2}} g_{ff} \exp\{-\frac{E}{kT_e} - K(E)D_n\}. \tag{3}$$

Therefore, total intensity I_n of x-ray transmitted through the foil is

$$I_n = \int_0^\infty I_E' \, dE \tag{4}$$

The total intensity ratio transmitted through the metal foils of thickness D_1 and D_2 is

$$\frac{I_2}{I_1} = \frac{\int_0^\infty \exp\{-E/kT_e - K(E)\ D_2\}dE}{\int_0^\infty \exp\{-E/kT_e - K(E)\ D_1\}dE} \tag{5}$$

The relations between the absorption coefficient K(E) and the energy of x-ray for Be foils of different thickness are shown in Fig.3. The relations between the intensity ratio of x-ray and electron temperature are shown in Fig.4, calculated by the authors. Electron temperatures were directly obtained from these data. A typical detected signal of x-ray is shown in Fig.5. The electron temperatures of several targets of $(CH_2)_n$, Be and C depended upon the laser powers are shown in Fig.6(a), (b) and (c) respectively. The electron temperature had a dependence on laser power p as $p^{2/3}$ for $(CH_2)_n$, $p^{4/9}$ for Be and $p^{2/9}$ for C, respectively.

No influence of laser pulse duration to the electron temperature was observed in the cases of durations 2.0 ns, 4 ns and 10 ns, but the intensity of x-ray increased for the longer pulse durations. The pulse duration of effective heating of plasma was less than 2 ns. The longer part of pulse energy was transferred to plasma propulsion and not to heating.

Electron temperatures with the laser input power of 200 MW were about 70 eV for $(CH_2)_n$, 100 eV for Be and 120 eV for C. The last one had the highest temperature at lower laser power but the increasing rate of electron temperatures was slow with increasing the laser power.

The intensity of x-ray from the Be plasma transmitted through the Be foil is shown in Fig.7. The solid lines are experimental values and dashed lines are theoretical ones, which were calculated from Eq.4, putting n_e and n_i = 10^{21} cm^{-3} (cut-off density), z = const. and using the elec-

tron temperature in Fig.6(b). The experimental values showed the incresing rate of x-ray for increasing laser power larger than the calculated ones. This is caused by the fact that the plasma volume or the particle number was increased as the laser power increased. The estimated particle number normalized by the value of the laser power of 1 GW is shown in Fig.8. The particle number increased remarkably for the increase of laser power.

(2) Measurements of incident and reflected laser beam.

Some amount of the input laser energy was reflected at the target. The pulse form of the incident and reflected laser light were measured by a same biplaner photodiode (HTV-R317) as shown in Fig.9. The time variations of reflectivity of laser power from the targets of Be and C with the incident power density $6 \times 10^{11} W/cm^2$ are shown in Fig. 10(a) and (b), respectively. Larger reflection was observed within the first 2 ns of incident laser pulse and thereafter, the reflection went down rapidly. This seems to be due to the increasing of the absorbing thickness of plasma with time. The reflectivity was 2 % for Be and 0.14 % for C. For the case of polyethylene target at the input power density about 6×10^{11} W/cm^2, the oscillation of the reflected laser light was observed at the electron temperature about 200 eV in Fig.11. The frequency was about 1.4×10^9 Hz. This may be caused by the beat of ion acoustic wave[8,9] induced by laser beam.

(3) The time of flight measurement of ions.

As ions occupy the greater part of energy in laser-produced plasma, it is very important to know ion temperature, density (ion number) and kinetic energy for investigation of heating of plasma. Especially, ion temperature in laser-produced plasma has not been reported in detail in spite of the many results on the electron temperatures. Ion temperatures of laser-produced plasma were estimated from ion velocity profile in the time fo flight measurements assuming the Maxwellian velocity distribution.[10,11] The ion collected by a charge collector through a very small entrance slit has one-dimensional Maxwellian velocity distribution. The velocity distribution function is given by

$$f(v) \propto \exp\{-\frac{m_i(v - v_d)^2}{2kT_i}\} \quad ,$$

where v_d is the drift velocity of ions and m_i is ion mass. Therefore the ion temperature is given by

$$kT_i = \frac{1}{2} m_i (\Delta v)^2 \quad ,$$

where Δv is a velocity spread corresponding to 1/e of the peak value of Maxwellian velocity distribution as shown in Fig.12. The ion velocity profile was measured by a Faraday cage with the ion-selecting grid and an electrostatic energy analyzer as shown in Fig.13 and Fig.14 respectively. In Fig.13, G_1 is an electron repelling grid, G_2 is a grounded grid, G_3 is an ion selecting grid and G_4 is a suppresser grid for secondary electron from the collector by ion

bombardment. When a positive voltage V is applied to grid G_3, ion whose velocity is larger than $v_0 = \sqrt{\frac{2zeV}{m_i}}$ can be collected, where m_i is the ion mass and z is charge number. The drift velocity of ion was known by the time of flight. When a certain voltage V_1 is applied, only Be^+ ion are collected in the time-of-flight range of $\ell/\sqrt{\frac{4eV_1}{m_i}} < t_1 < \ell/\sqrt{\frac{2eV_1}{m_i}}$, two species of Be^+ and Be^{2+} ions are collected in $\ell/\sqrt{\frac{6eV_1}{m_i}} < t_2 < \ell/\sqrt{\frac{4eV_1}{m_i}}$, Be^+, Be^{2+} and Be^{3+} ions in $\ell/\sqrt{\frac{8eV_1}{m_i}} < t_3 < \ell/\sqrt{\frac{6eV_1}{m_i}}$ and Be^+, Be^{2+}, Be^{3+} and Be^{4+} ions in $t_4 < \ell/\sqrt{\frac{8eV_1}{m_i}}$ respectively, where ℓ is the distance from target to collector. As the voltage increased, the time-of-flight ranges and collected ion signals were varied and thus species of ions were discriminated. The current signal of collected ions were shown in Fig.15(a), (b) and (c) for the different voltages of the grid; 0, 200, 250 V, respectively. A relation between the species of collected ions and time of flight is shown in Fig.15(d).

Using the electrostatic energy analyzer as shwon in Fig.14, ion of the velocity v corresponding to the relation $mv^2/r = zeV/d$ can be collected where m, z are ion mass and charge number, respectively and d, r are space between the electrodes and the radius of curvature of the analyzer and V is an applied voltage. Putting $\ell = vt$, the time of flight is $t = \sqrt{\frac{m}{e}} \cdot \sqrt{\frac{d}{r}} \cdot \ell \cdot \frac{1}{\sqrt{z}} \cdot \frac{1}{\sqrt{V}}$. This is inversely proportional to the square root of the charge number z and the voltage V for the ion of same value of m/e. The velocity profile of ion was obtained by scanning of the voltage V. The typical

signals of ions were shown in Fig.16. The ion velocity distributions of Be plasma were shown in Fig.17 in the laser power range of 470 ∿ 625 MW. They were approximately Maxwellian. The ion temperature and drift velocity obtained from these velocity distribution were shown in Table I.[12] Electron temperatures obtained from the soft x-ray measurement were about 130 eV for the same laser power range. The numbers of higher multicharged ion were larger than that of lower charged ones and the former ions had higher temperature and the higher charged ions had larger drift velocity than lower charge one as shwon in Fig.17 and Table I. Using a slow rising laser beam, whose rise time was 10 ns, the above mentioned characteristics became in the reverse sense.[11,13]

From our experimental results the effective heating time of plasma was less than 2 ns and the plasma expanded semi-spherically with the average velocity of 2×10^7 cm/sec.

From the experiment of the shadowgraph the radius of the plasma was about 0.2 mm at the end of heating. The plasma density estimated from collected ion current was about 6×10^{19} cm^{-3}. The number of plasma particles in a sphere was about 10^{15}. Thus the total energy of plasma was estimated about 0.2 J.

If this energy is initially absorbed by electrons, the mean energy of an electron is up to about 2.5 keV. Therefore, Be^{4+}, the ionization energy of which is 218 eV, can be easily produced. From the reflection measurement of input laser beam the laser energy seems to be fully absorbed in plasma. While the above estimated energy was about one-fourth of the incident laser energy. This might be due to the

ambiguity of the collected ion density of plasma.

4. Discussions

Experimental results showed that the effective heating was done in 2 ns at the beginning of incident laser pulse. After this period, the expansion of plasma was introduced. The electron heating in the range of the laser power 10^{12} W/cm^2 are caused by the classical inverse bremsstrahlung. The energy relaxation time τ_{ei} by the collision of ion and electron and the expansion characteristic time τ_s are given by

$$\tau_{ei} = \frac{3}{8\sqrt{2}\pi} \frac{m_i (kT_e)^{3/2}}{m_e^{1/4} e^4 z^2 n_e \ell n\Lambda} \sim \frac{3 \times 10^9 A\, T_e^{3/2}}{n_e z^2 \ell n\Lambda}$$

$$\tau_s = \frac{x_0}{V_s} = x_0 \left(\frac{5kT_e}{3m_i}\right)^{-1/2} = \frac{x_0 \sqrt{A}}{1.3 \times 10^6 T_e^{1/2}}$$

where m_i, m_e are ion and electron mass, z is charge number, n_e is electron density, A is atomic mass number and x_0, V_s are a plasma dimension, the order of 10^{-2} cm and sound velocity, respectively.

When an inequality $\tau_{ei} < \tau_s$ holds, the effective heating of ions by energy relaxation from electrons is performed.[14] The electron temperature T_e^* at $\tau_{ei} = \tau_s$ gives a measure of relaxation by the laser pulse width of effecting heating.

T_e^* and τ_s are given by

$$T_e^* = \frac{5 \times 10^{-8} z (n_e x_0 \ell n\Lambda)^{1/2}}{A^{1/4}} \sim 1 \text{ keV}$$

$$\tau_s \sim 0.7 \text{ ns}$$

at $n_e \sim 10^{21}$ cm^{-3}, x_0 = 100 μ and A = 9 (Be). Therefore it is theoretically possible to heat a plasma up to 1 keV for the Be target by a high power nanosecond laser pulse. As shown in Fig.6(b), the electron temperature of Be plasma was 100 to 200 eV. τ_s was about 1.6 ns in this temperature range, which was consistent with the used laser pulse 2 ns. The dependency of electron temperature on the incident laser power varied remarkably for different species of target as shown in Fig.6(a), (b) and (c). The electron temperature of polyethylene $(CH_2)_n$ plasma accorded very well with the theoretical estimation considering hydrodynamic expansion of plasma with classical heating ($T_e \sim P^{2/3}$).[15] But those of Be and C plasma differed from this characteristic and showed the considerably lower increasing rate of electron temperature.[16] The energy relaxation time τ_{ei} of $(CH_2)_n$, Be^{4+} and C^{6+} were 3.8, 3.0 and 1.9 × 10^{-11} sec respectively where average charge number and atomic mass number were used in $(CH_2)_n$ ions. The electron temperature in carbon plasma was lowered most rapidly than any other plasma by energy relaxation of electron and ion. The ionization potentials of $(CH_2)_n$ ions, Be^{4+} and C^{6+} are 172, 218 and 490 eV respectively where the average ionization potential was used in $(CH_2)_n$ ion. The carbon target needs higher energy to be ionized. As C and Be are good thermal conductor compared with $(CH_2)_n$, much more neutral particles can be evaporated in C and Be than in $(CH_2)_n$.[17] Indeed different type of crater was created around the focal spot in Be and C compared with $(CH_2)_n$. Thus the characteristics of electron temperatures in Be and C seems to be caused by the different dissipations of laser

power from $(CH_2)_n$.

As shown in Fig.10(a) and (b), larger reflection occurred in about 2 ns at the beginning of incident laser pulse. This seems to be caused by the fact that in the focal spot region a sharp boundary layer whose density was close to cut-off density was formed at the early period of laser irradiation and then by the expansion of plasma the density decreased to absorb the laser power.

When the fast rising pulse whose rise time was about 1 ns and power was 1 GW was used, fully ionized plasmas was produced in the focal spot. In this case Be^{4+} ion was produced at the front of the pulse and the lower ionized ions of Be seemed to be yielded after the peak of the pulse.

As shown in Fig.17, Be^{+} ions which had especially low temperature and small number were produced by the tail of the laser pulse possibly because of ionization potential being low ($\sim$ 9.4 eV). For the plasma expanding with velocity of the order of 10^7 cm/sec electron temperature of more than 100 eV, the recombination was not important[18] and the velocity profile of the time of flight measurement represented the velocity distribution of the relaxed plasma between electron and ions. The number of higher charged ions was larger than that of lower charged ones and the former has higher temperature and larger drift velcity. As energy relaxation time by collision of electron and ion is inversely proportional to z^2, higher charged ion was heated more effectively than lower charger ions.

The electrons are inclined to escape out of the plasma sphere, building up an electrostatic field. This field

accelerates the remaining ions proportional to their charge z. This collective process may induce the resulting kinetic energy of ions much higher than that of low z ions. For the slow rising laser pulse whose rise time was 10 ns, few higher ionized ions were produced and most of ions were lower ionized ones. The temperature of the latter was higher than that of the former.[13,15] Thus above mentioned characteristics, which were varied by the rise times, depend on whether the incident laser energy was absorbed effectively or not before the expansion of plasma.

5. Conclusions

We have performed the preliminary experiments on high z materials to clarify the heating mechanism of plasma by laser. In this paper the laser power was restricted up to 1 GW, the power density 10^{12} W/cm^2, so the classical heating was mainly operative.

The several points clarified by the experiments are the followings:

(1) The effective heating of plasma occurred in about 2 ns of the beginning of incident laser pulse. Thereafter, incident laser energy was transferred to kinetic energy and to the increase of the number of particles.

(2) Laser power dependency of electron temperature varied remarkably for the species of targets. That of polyethylene $(CH_2)_n$ was consistent with results estimated by a simple hydrodynamic expansion treatment with the classical heating $T_e \sim P^{2/3}$. But those of beryllium and carbon were not consistent with this law. This difference of dependency was

explained qualitatively by the difference of energy dissipation in producing plasma.

(3) The plasma produced by fast rising laser pulse and by slow rising one had quite different characteristics: (a) In the former the number of ions with higher z numbers was much larger than that with lower z numbers because the fairly amount of incident laser energy was fed into plasma before the expansion. On the other hand, in the latter, highly ionized ions were scarcely produced and ions with lower z numbers were dominant as the plasma expanded during the laser pulse. (b) In the former, highly ionized ions had higher temperature than those with lower z numbers, while this is opposite in the latter case.

(4) The reflection of laser light from plasma depends on formation of plasma layer. The reflectivity was larger in about 2 ns at the beginning of incident laser pulse than the later period.

Increasing the laser power, we are planning to investigate the anomalous heating effects in high z plasmas.

Acknoledgements

The authors are very grateful to the Tore Science Promotion Society and also the Minister of Education for scientific research funds. The authors also express their sincere thanks to Professor K. Husimi and Professor K. Takayama for their encouragement.

And the authors wish to acknowledge with Mr. N. Miyajima for the assistance of experiments.

References

1) W. I. Linlor: Appl. Phys. Lett. 3, 210 (1963)

2) B. E. Paton and N. R. Isener: Can. J. Phys. 46, 1237 (1968)

3) M. Onishi and C. Yamanaka: Technol. Rep. Osaka Univ. 20, 121 (1970)

4) J. F. Ready: Appl. Phys. Lett. 3, 11 (1963)

5) N. G. Basov, O. N. Krokhin et al.: Appl. Opt. 6, 1814 (1967)

6) K. Yoshida, T. Yamanaka, T. Sasaki, H. Kang, M. Waki and C. Yamanaka: Japan. J. appl. Phys. 10, 1643 (1971)

7) R. C. Elton and A. D. Anderson: NRL Report 6541 (1967) Naval Research Lab., Washington

8) M. Waki, T. Yamanaka, H. Kang, K. Yoshida and C. Yamanaka: Japan. J. appl. Phys. 11, No.3 (1972)

9) K. Nishikawa and Y. Ichikawa: Phys. of Fluids 12, 2563 (1969)

10) P. Langer et al.: IEEE J. Quant. Electron. QE-2, 499 (1966)

11) F. J. Allen: J. Appl. Phys. 41, 3048 (1970)

12) H. Kang, T. Yamanaka, K. Yoshida, M. Waki and C. Yamanaka: Japan. J. appl. Phys. 11 765 (1972)

13) M. Mattioli and D. Veron: Panel 3.2.6 "Laser Induced Discharge" 332 (1970)

14) N. G. Basov et al.: Quantum Radio Phys. Lab. Preprint No.60 (1970)

15) C. Fauquignon and F. Floux: Phys. of Fluids 13, 386 (1970)

16) A. Caruso: LGI 70/12/E Sept., 1970

17) Y. Izawa and C. Yamanaka: Japan. J. appl. Phys. 7 954 (1968)

18) M. Mattioli: Plasma Phys. 13, 19 (1971)

Figure Captions

Fig.1 Experimental arrangement of laser plasma research. R: rotating Q-switched glass laser (2 ns, 9 mJ), GP: Gran prism, PC: Pockels cell, LTSG: laser triggered spark gap, DC: Saturable dye cell, Amp.I∿V: Amplifier stage, US: uniguide slit, P: polarizer, FR: Faraday rotator, BS: beam splitter, A: attenuator, M: mirror, XD: x-ray detector, FC: Faraday cage, Spec.: spectrometer, He-Ne: He-Ne laser

Fig.2 X-ray detector.

Fig.3 Absorption coefficeint of Be foils of different thickness vs. energy of x-ray.

Fig.4 Intensity ratio of x-ray transmitted through Be foil vs. electron temperature.

Fig.5 Typical x-ray signal.

Fig.6 (a) Electron temperature of $(CH_2)_n$ plasma with incident laser power. (b) Electron temperature of Be plasma with incident laser power. (c) Electron temperature of C plasma with incident laser power.

Fig.7 Intensity of x-ray transmitted through Be foil with incident laser power. Solid line: experimental value. Dashed line: theoretical value.

Fig.8 Number of particles with incident laser power.

Fig.9 Experimental arrangement for measurement of incident and reflected laser beam.

Fig.10 Incident and reflected laser power, reflectivity vs. time. (a) Be target, (b) C target.

Fig.11 Incident and reflected laser light.

Fig.12 Temperature determination from Maxwell velocity distribution.

Fig.13 Faraday cage with ion selecting grid.

Fig.14 Electrostatic energy analyzer.

Fig.15 Typical signals of collected ions of Faraday cage.

Fig.16 Typical signals of collected ions of electrostatic energy analyzer (upper trace). Monitor signal (lower trace).

Fig.17 Ion velocity distribution of Be plasma. Laser pulse width: 4 ns.

Table Caption

Table I. Ion temperature and drift velocity.

Table I

Ion Species	Laser Power (MW)	Ion Temp. (eV)	Drift Velocity & Drift Energy ($\times 10^7$ cm/sec)	(keV)
Be^{+}	215 ± 25	few	0.90	0.38
Be^{2+}		27	1.25	0.73
Be^{3+}		75	1.64	1.30
Be^{4+}		100	2.15	2.20
Be^{+}	550 ± 70	few	1.10	0.57
Be^{2+}		32	1.60	1.20
Be^{3+}		120	2.15	2.20
Be^{4+}		120	2.55	3.00

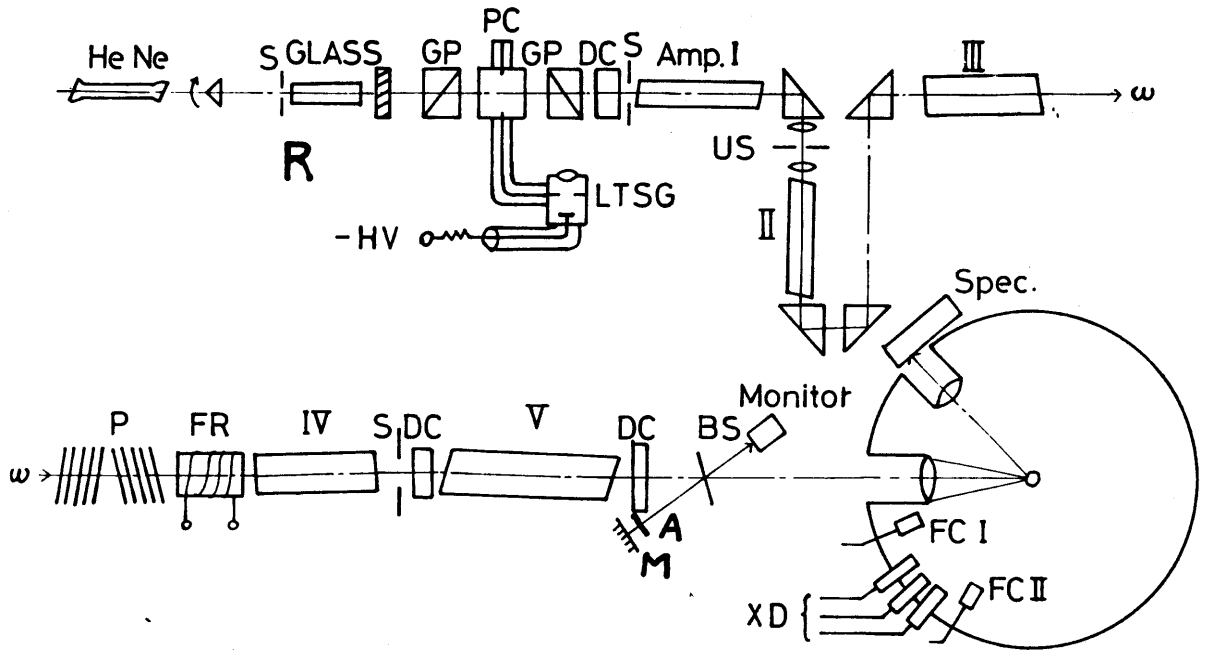
He Ne
S
GLASS
GP
PC
GP
DC
S
Amp. I
III
ω
R
US
LTSG
-HV
II
Spec.
Monitor
P
FR
IV
S
DC
V
DC
BS
ω
A
M
FC I
FC II
XD

Fig. 1

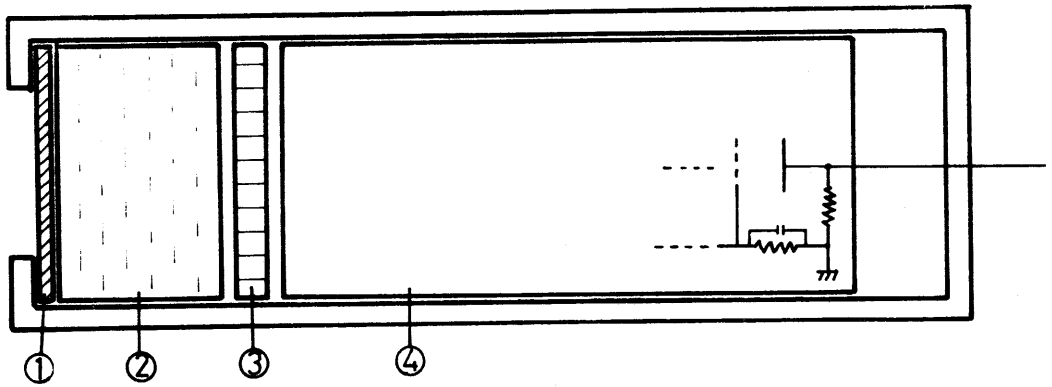

X-ray Detector

1. Absorber (Be : 25μ , 100μ), 2. Plastic scintillator
3. Neutral density filters , 3. Photomultiplier (HTV - R 292)

Fig. 2

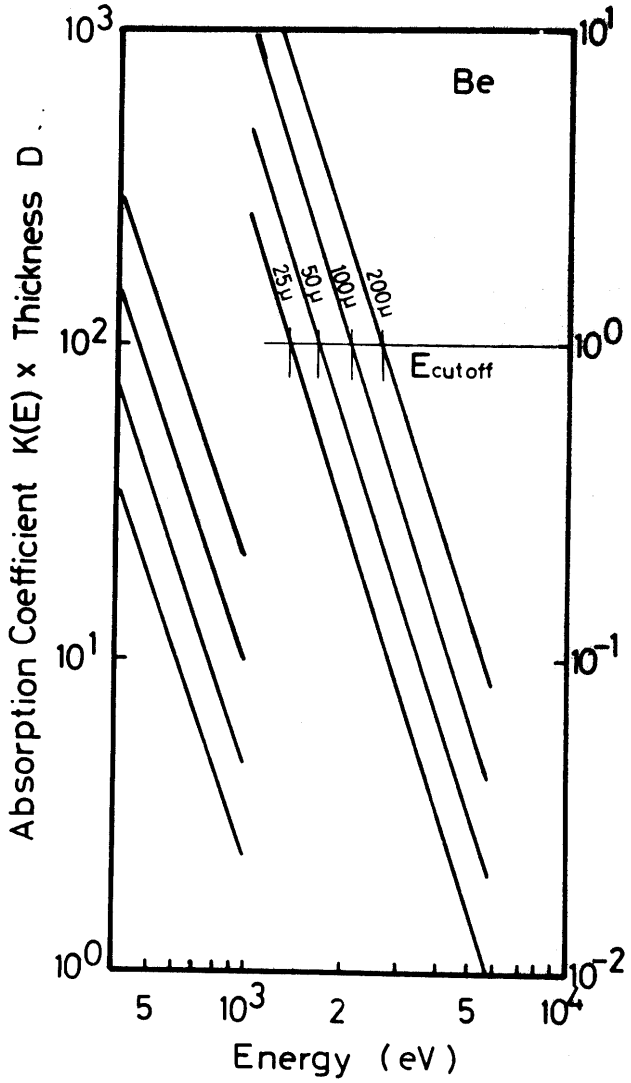
Be
Absorption Coefficient K(E) x Thickness D
Energy (eV)
Ecutoff
25μ
50μ
100μ
200μ
10^3
10^2
10^1
10^0
10^1
10^0
10^-1
10^-2
5
10^3
2
5
10^4

Fig. 3

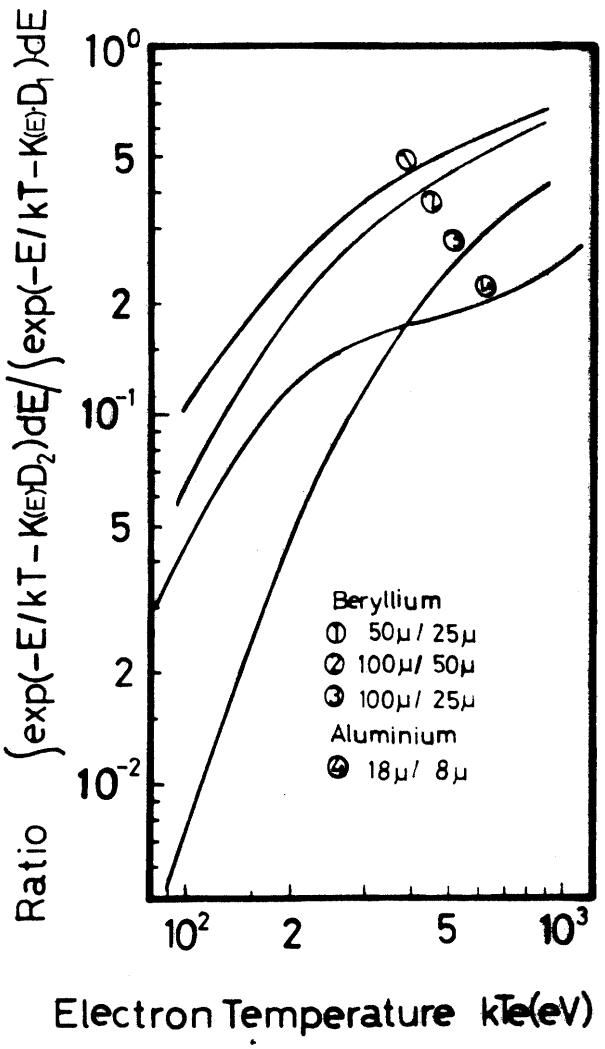
Ratio ∫exp(-E/kT-K(E)D2)dE/∫exp(-E/kT-K(E)D1)dE
10^0
5
2
10^-1
5
2
10^-2
10^2
2
5
10^3
Electron Temperature kTe(eV)
Beryllium
① 50μ/ 25μ
② 100μ/ 50μ
③ 100μ/ 25μ
Aluminium
④ 18μ/ 8μ

Fig. 4

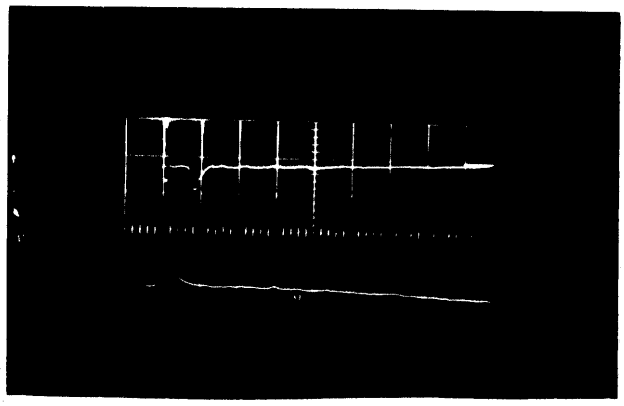

Be 100 μ

Be 25 μ

X-ray Signal (100 ns / div)

Fig. 5

(a)

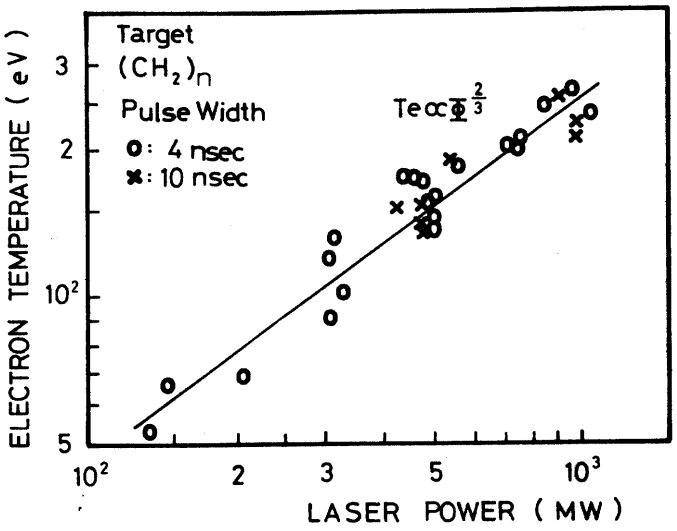
Target
$(CH_2)_n$
Pulse Width
o: 4 nsec
×: 10 nsec
$Te \propto \Phi^{\frac{2}{3}}$
ELECTRON TEMPERATURE (eV)
LASER POWER (MW)

(b)

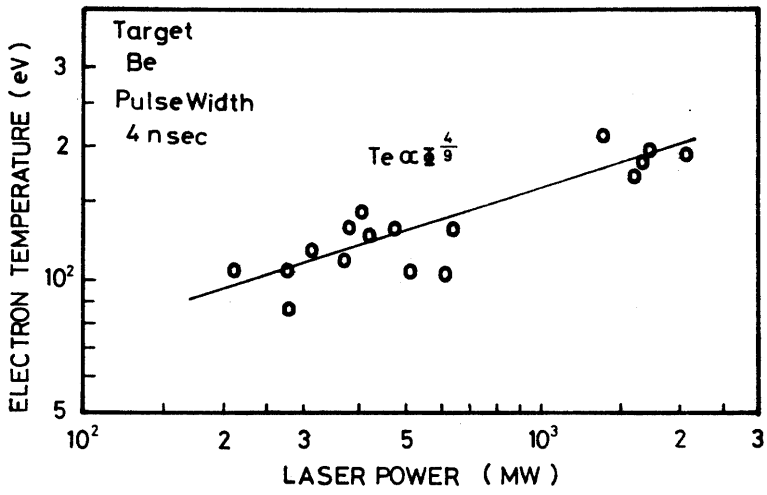
Target
Be
Pulse Width
4 nsec
$Te \propto \Phi^{\frac{4}{9}}$
ELECTRON TEMPERATURE (eV)
LASER POWER (MW)

(c)

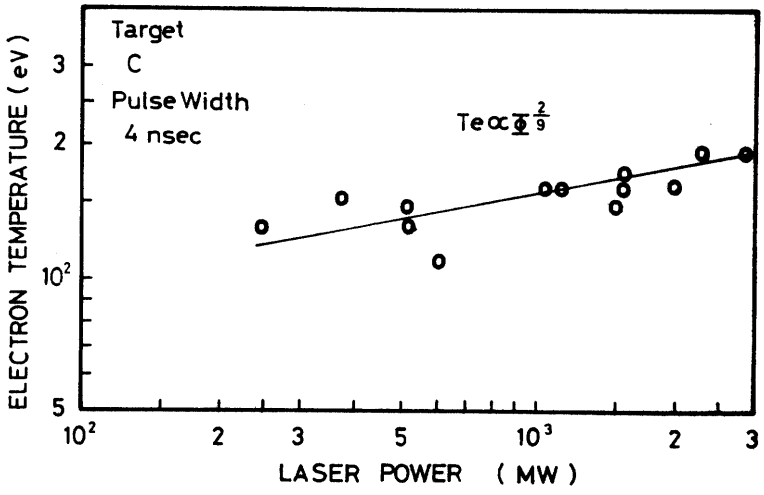
Target
C
Pulse Width
4 nsec
$Te \propto \Phi^{\frac{2}{9}}$
ELECTRON TEMPERATURE (eV)
LASER POWER (MW)

Fig. 6

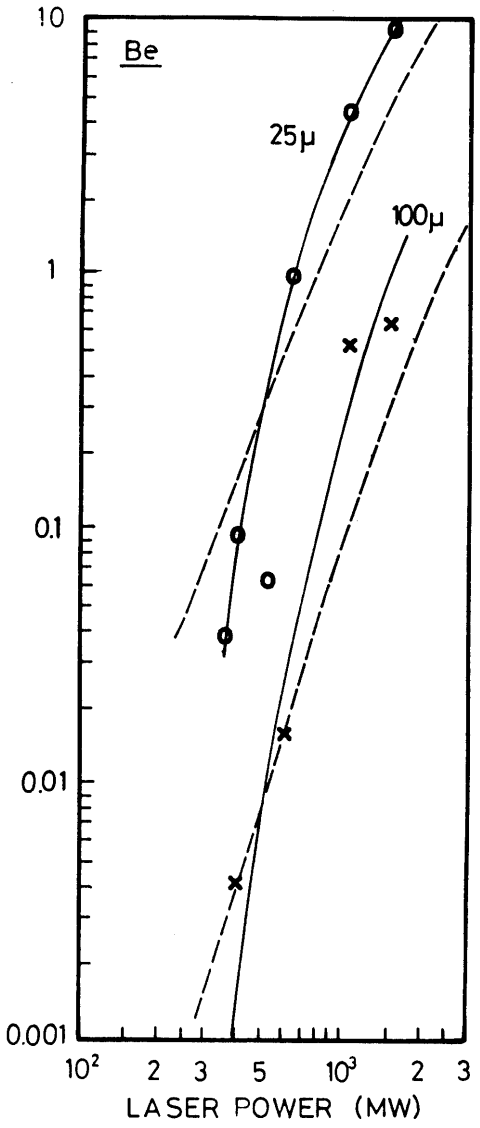

Fig. 7

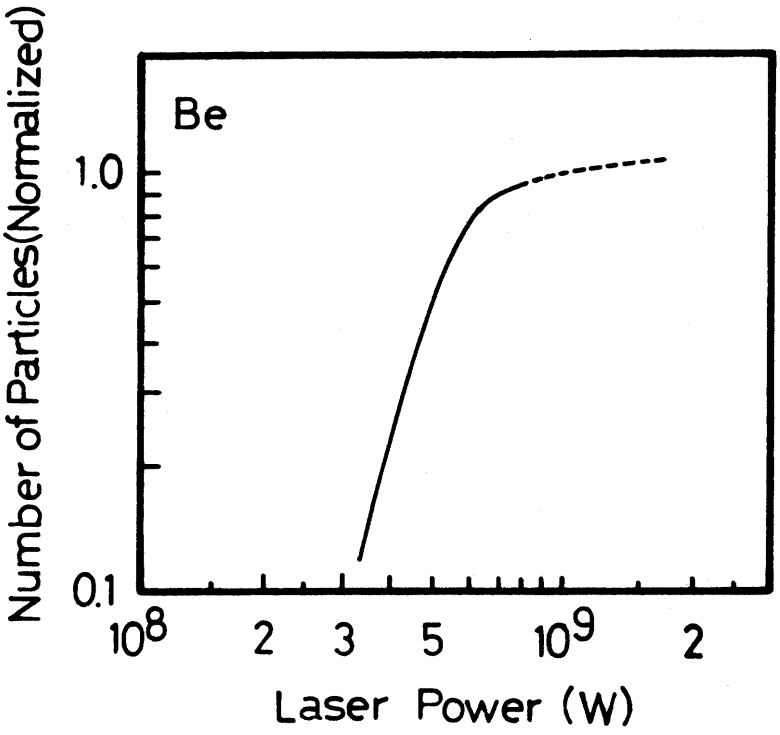
Be
1.0
0.1
Number of Particles(Normalized)
10^8
2
3
5
10^9
2
Laser Power (W)

Fig. 8

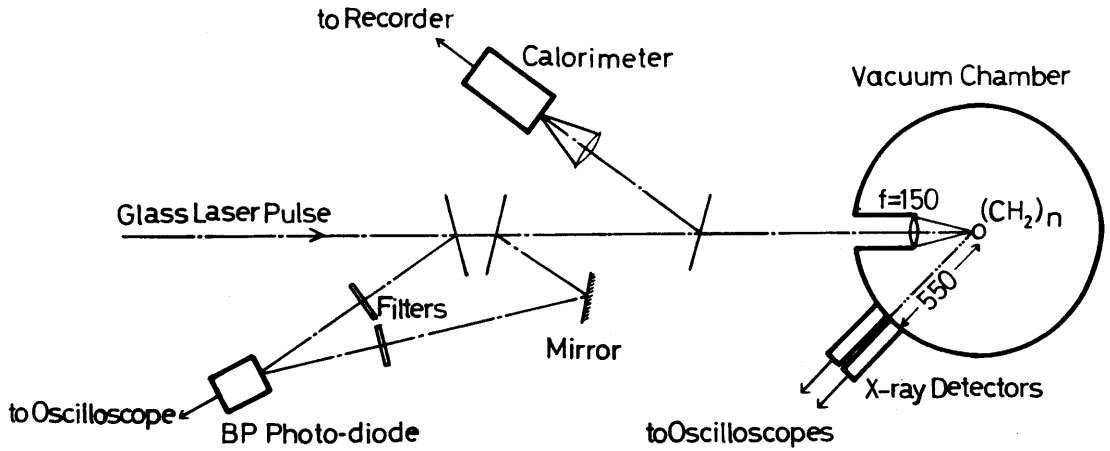
to Recorder
Calorimeter
Vacuum Chamber
Glass Laser Pulse
f=150
$(CH_2)_n$
Filters
Mirror
550
X-ray Detectors
to Oscilloscope
BP Photo-diode
to Oscilloscopes

Fig. 9

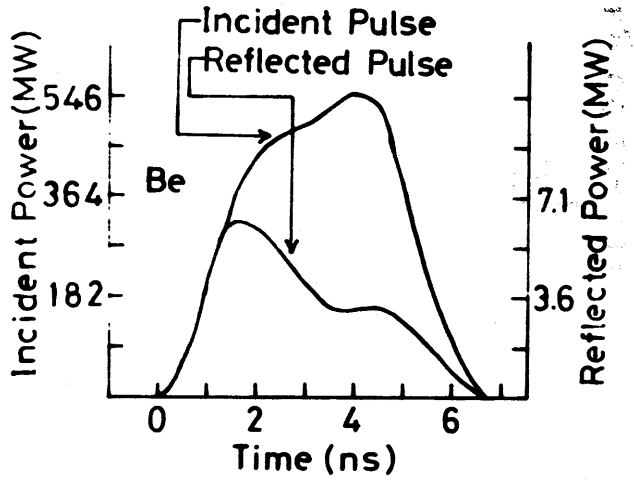
Incident Pulse
Reflected Pulse
Incident Power(MW)
546
364
182
Be
7.1
3.6
Reflected Power(MW)
0
2
4
6
Time (ns)

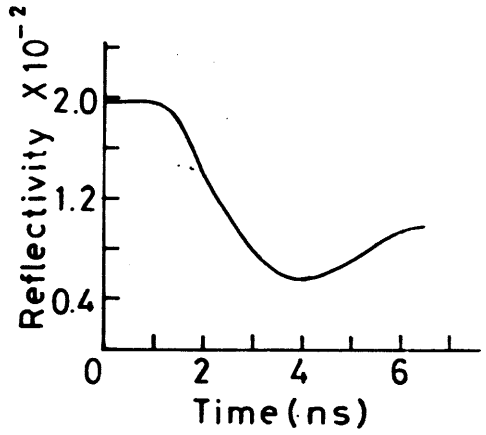
Reflectivity X10⁻²
2.0
1.2
0.4
0
2
4
6
Time(ns)

(a)

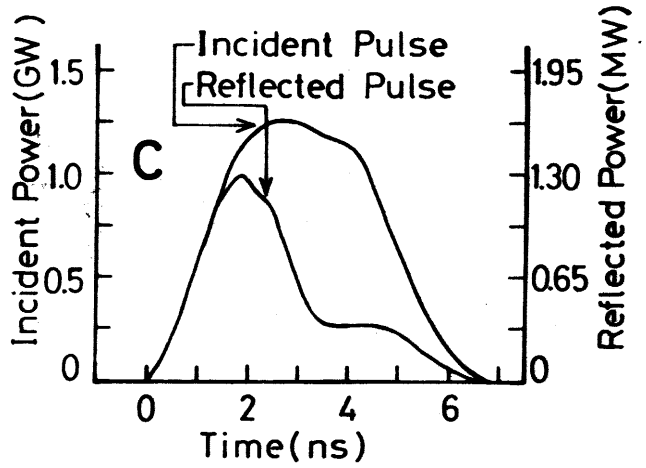
Incident Pulse
Reflected Pulse
Incident Power(GW)
1.5
1.0
0.5
0
C
1.95
1.30
0.65
0
Reflected Power(MW)
0
2
4
6
Time(ns)

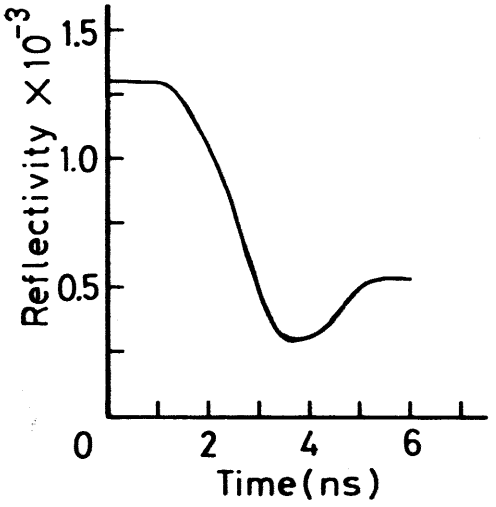
Reflectivity X10⁻³
1.5
1.0
0.5
0
2
4
6
Time(ns)

(b)

Fig. 10

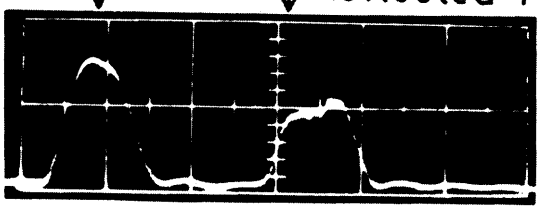
Incident Pulse
Reflected Pulse
5 ns/div
Target
$(CH_2)_n$
Power Density
6×10^{11} W/cm^2
Incident —
Reflection Ratio
$\frac{1}{100}$

Fig. 11

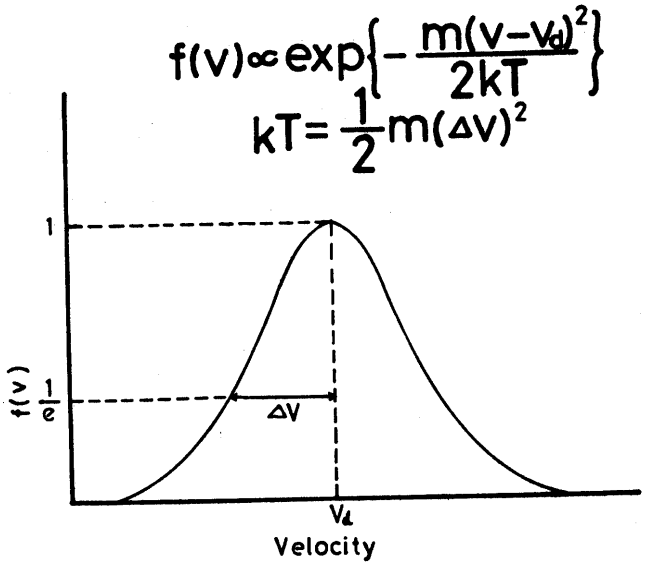
$f(v) \propto \exp\left\{-\frac{m(v-v_d)^2}{2kT}\right\}$
$kT = \frac{1}{2}m(\Delta v)^2$
1
$f(v)\ \frac{1}{e}$
ΔV
V_d
Velocity

Fig. 12

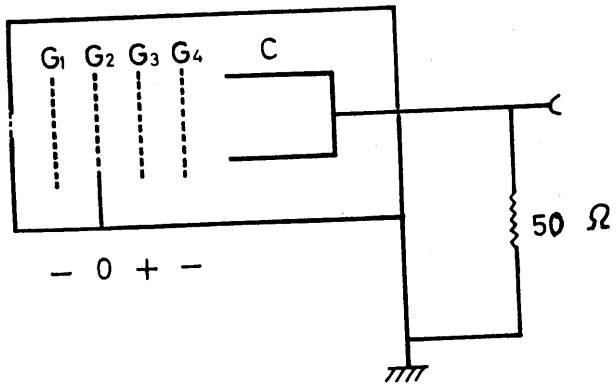

G_1: Electron Repelling Grid
G_3: Ion Selecti ng Grid
G_4: Suppressing Grid for Secondary Electron

Fig. 13

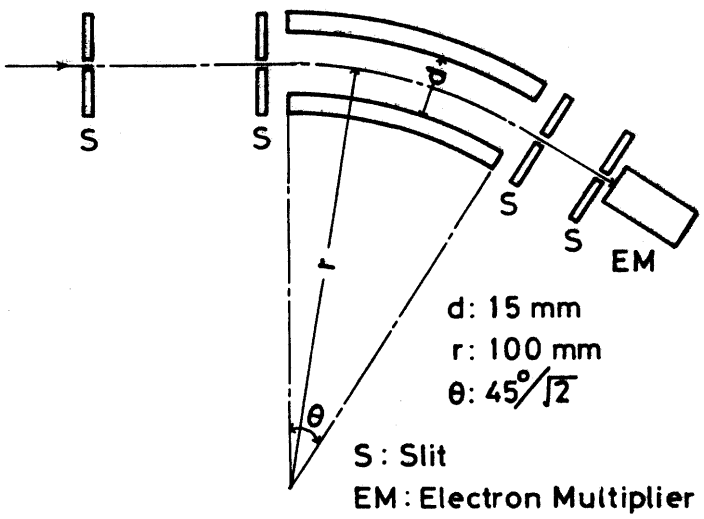

Fig. 14

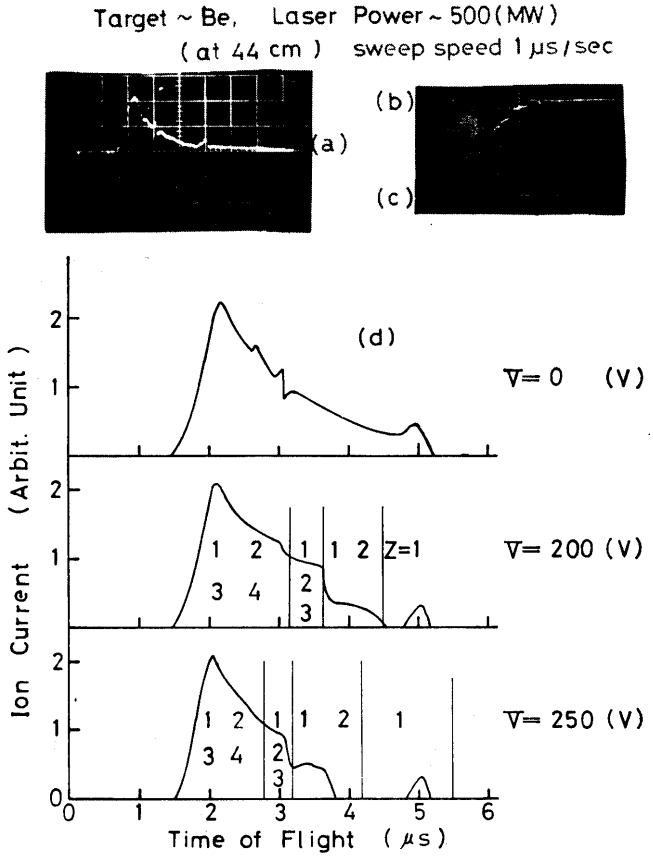
Target ~ Be, Laser Power ~ 500 (MW)
(at 44 cm) sweep speed 1 μs / sec
(a)
(b)
(c)
(d)
V= 0 (V)
V= 200 (V)
V= 250 (V)
Z=1
Ion Current (Arbit. Unit)
Time of Flight (μs)

Fig. 15

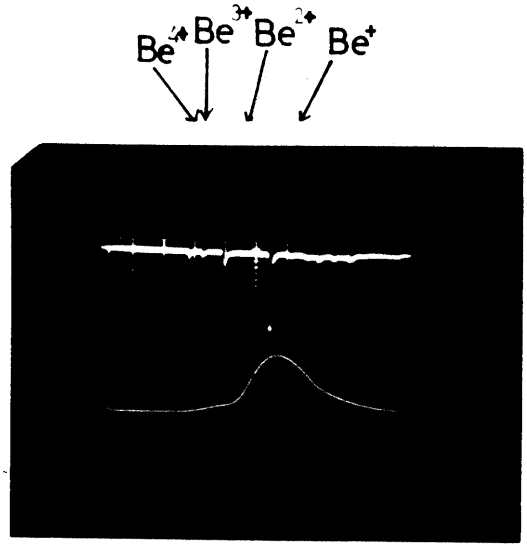

L : 81.5 cm L.I.P. : 400 MW

0.05 V/div. 0.5 μs/div.

Be^{4+} ~ 3.0 KeV

Be^{3+} ~ 2.25

Be^{2+} ~ 1.5

Be^{+} ~ 0.75

Fig. 16

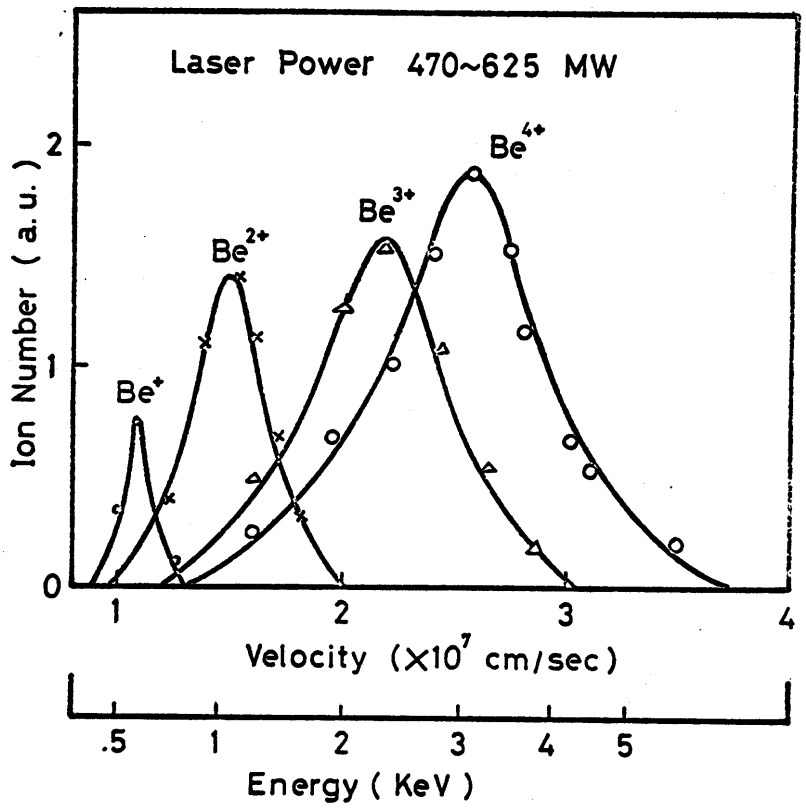
Laser Power 470~625 MW
Ion Number (a.u.)
2
1
0
Be+
Be2+
Be3+
Be4+
1
2
3
4
Velocity (X10^7 cm/sec)
.5
1
2
3
4
5
Energy (KeV)

Fig. 17